ORIGINAL ARTICLE

A pair of new enantiomeric hybrid phthalide–adenines with a rare 5-oxa-1-azaspiro[3,4]octane moiety and two pairs of new enantiomeric hybrid paraethyl phenol–adenines from *Ligusticum chuanxiong*

Rui Feng [a,b,c,1], **Juan Liu** [a,b,c,1], **Li Guo** [a,b,c,*], **Hong-Zhen Shu** [a,b,c], **Qin-Mei Zhou** [a,c], **Li Liu** [d], **Cheng Peng** [a,b,*], **Liang Xiong** [a,b,c,*]

[a] *State Key Laboratory of Southwestern Chinese Medicine Resources, Chengdu University of Traditional Chinese Medicine, Chengdu 611137, China*
[b] *School of Pharmacy, Chengdu University of Traditional Chinese Medicine, Chengdu 611137, China*
[c] *Institute of Innovative Medicine Ingredients of Southwest Specialty Medicinal Materials, Chengdu University of Traditional Chinese Medicine, Chengdu 611137, China*
[d] *Chiataj Qingchunbao Pharmaceutical Co., Ltd, Hangzhou 310023, China*

Abstract Three pairs of new enantiomeric adenine alkaloids, $(+)/(-)$-liguadenines A–C [$(+)/(-)$-**1**–**3**], were isolated from the rhizome of *Ligusticum chuanxiong* Hort. The structures and absolute configurations of these compounds were determined using spectroscopic data, single-crystal X-ray diffraction, and electronic circular dichroism analyses. To the best of our knowledge, compounds $(+)$-**1** and $(-)$-**1** are the first hybrid phthalide–adenines to be ever reported. The linkage between the phthalide and adenine units in these compounds forms a rare 5-oxa-1-azaspiro[3,4] octane moiety. Analyses of the anti-inflammatory activities of the isolated compounds show that $(+)/(-)$-**1** and $(+)$-**3** exhibit significant inhibitory activity against LPS-induced TNF-α and IL-6 production in RAW264.7 cells. RT-qPCR analysis confirms that the most active compound,

* Corresponding authors at: State Key Laboratory of Southwestern Chinese Medicine Resources, Chengdu University of Traditional Chinese Medicine, Chengdu 611137, China.
 E-mail addresses: guoli@cdutcm.edu.cn (L. Guo), pengcheng@cdutcm.edu.cn (C. Peng), xiling@cdutcm.edu.cn (L. Xiong).
 [1] Both authors contributed equally to this work.

(+)-**3**, exerts anti-inflammatory activity by downregulating the mRNA expressions of TNF-α and IL-6 in the cells.

1. Introduction

The rhizome of *Ligusticum chuanxiong* Hort. (synonyms *L. striatum* DC.) (Apiaceae), used as medicine for nearly 2,000 years in China, plays an important role in clinical practice due to its remarkable effects in promoting blood circulation and removing blood stasis (Chen et al., 2018). Thus far, various types of secondary metabolites, such as phthalides (Huang et al., 2022, Zhang et al., 2020, Zhang et al., 2021), alkaloids (Pu et al., 2022, Zhang et al., 2018a), polysaccharides (Wang et al., 2022, Wang et al., 2019), and organic acids (Chen et al., 2018, Zhang et al., 2018b), have been detected in *L. chuanxiong*. In light of their significant and effective biological activities, the phthalides and alkaloids extracted from *L. chuanxiong* have attracted great attention. The phthalides, a major class of secondary metabolites in *L. chuanxiong*, exhibit excellent anti-platelet aggregative, anticoagulant, vasorelaxant, and uterine smooth muscle relaxant activities (Chen et al., 2018, Huang et al. 2022, Liu et al., 2022), whereas the alkaloids, including pyrazines, carbolines, adenines, nucleosides, and phenylpropanoid-amino acid adducts, exhibit significant antiplatelet aggregative and anti-cerebral ischemia reperfusion injury activities (Pu et al., 2022, Zhang et al., 2018a).

Adenine, an important natural alkaloid, has been used as a scaffold for the synthesis of many medicinal compounds, such as fludarabine, cladribine, adefovir, and tenofovir (Buyens et al., 2017, Goswami et al., 2017, Luo et al. 2018). Adenine derivatives, most of which are substituted at N-9 or N-10 have also been detected in many plants. Although the N-9-substituted derivatives such as adenosine and nucleoside are much more common than the N-10-substituted counterparts (Araya et al., 2011, Bakr et al., 2021, Ma et al., 2008, Ma et al., 2007, Wang et al., 2021), we have succeeded in isolating two N-10-substituted nucleoside alkaloids from *L. chuanxiong* (Pu et al., 2019). We have also isolated butylphthalides, the most significant phthalides in *L. chuanxiong*, and phthalide dimers from this plant (Huang et al. 2022, Liu et al., 2022). However, phthalide–adenine hybridization has not yet been reported.

As part of our ongoing investigation regarding the rhizome of *L. chuanxiong*, three pairs of new enantiomeric adenine alkaloids (**1**–**3**) have been isolated in this study (Fig. 1), and their absolute configurations have been elucidated using X-ray diffraction analysis and electronic circular dichroism (ECD) calculations. Notably, (+)-**1** and (−)-**1** are the first hybrid phthalide–adenines to ever be reported. The linkage between the phthalide and adenine units in these compounds results in the formation of a rare 5-oxa-1-azaspiro[3,4]octane moiety that has been reported in four synthesis studies only (Cordero et al. 2011, Capraro et al., 1983, Shipov and Baukov, 1988, Roth, 1979). As for compounds (+)-**2**, (−)-**2**, (+)-**3**, and (−)-**3**, they are hybrid paraethyl phenol–adenines. Herein, the isolation method, structure, absolute configuration, and anti-inflammatory activity of rare hybrid adenines in *L. chuanxiong* are discussed.

2. Experimental

2.1. General experimental procedures

Optical rotations and IR data were measured using an Anton Paar MCP 200 automatic polarimeter (Anton Paar GmbH, Graz, Austria) and an Agilent Cary 600 FT-IR microscope (Agilent Technologies Inc., CA, USA). ECD spectra were recorded using an Applied Photophysics Chirascan and Chirascan-plus circular dichroism spectrometer (Applied Photophysics ltd., Leatherhead, England). NMR spectra were obtained by a Bruker-AVIIIHD-600 spectrometer or a Bruker Avance NEO 600 spectrometer (Bruker Corporation, Billerica, MA, USA) with solvent peaks as reference standards. X-ray structure analyses were performed on a Bruker D8 QUEST diffractometer (Bruker Corporation, Billerica, MA, USA). HRESIMS measurements were carried out using a Waters Synapt G2 HDMS instrument (Waters Corporation, Milford, MA, USA) or a Bruker tims-TOF-MS instrument (Bruker Corporation, Billerica, MA, USA). TLC was performed using glass plates precoated with silica gel GF_{254} (Qingdao Marine Chemical Inc., Qingdao, China). Column chromatography separation was performed using D-101-type macroporous adsorbent resin (Chengdu Kelong Chemical Reagent Factory, Chengdu, China), 732-type strong acid cation exchange resin (Chengdu Chron Chemicals Co., ltd., Chengdu, China), silica gel (200–300 mesh, Yantai Institute of Chemical Technology, Yantai, China), and Sephadex LH-20 (40–70 μm, Amersham Pharmacia Biotech AB, Uppsala, Sweden). Meanwhile, HPLC separations were carried out using an Alltech 426 instrument. Reversed-phase semipreparative HPLC analyses were conducted on a Zorbax SB-C_{18} (250 × 9.4 mm², 5 μm) column, while normal-phase and reversed-phase enantioseparations were conducted on Daicel Chiralpak AD-H (250 × 4.6 mm², 5 μm) and Daicel Chiralpak IG (250 × 4.6 mm², 5 μm) columns, respectively. The uterine smooth muscle relaxant activity and vasorelaxant activity of the isolated compounds were assessed using a PL3508B6/C-V Panlab 8 Chamber Organ Bath System (AD Instruments, Australia). RAW264.7 cells were obtained from Obio Technology Corp (Changsha, China), while the lipopolysaccharide was obtained from Sigma-Aldrich (St. Louis, MO, United States). Curcumin was purchased from Sichuan Weikeqi Biological Technology Co., ltd. (Sichuan, China). Mouse IL-6 Elisa and Mouse TNF-α Elisa kits were purchased from Elabscience Biotechnology Co., ltd. (Wuhan, Hubei, China). Total RNA Isolation Kit, 2 × RT OR-Easy™ Mix, and 2 × Real Time PCR Easy™ MIX-SYBR Green I were obtained from Chengdu Foregene Biological Technology Co., ltd. (Chengdu, China).

2.2. Plant material

Ligusticum chuanxiong Hort. was obtained from NeoGreen Pharmaceutical Technology Development Co., ltd. (Pengzhou, China) in October 2016. The sample was identified by Dr. Jihai Gao and deposited in the School of Pharmacy at Chengdu University of Traditional Chinese Medicine (specimen: LC-20161030).

2.3. Extraction and isolation

The *L. chuanxiong* rhizome (100 kg) was decocted with H_2O three times (2.5 h each time). The residue (28.8 kg) obtained
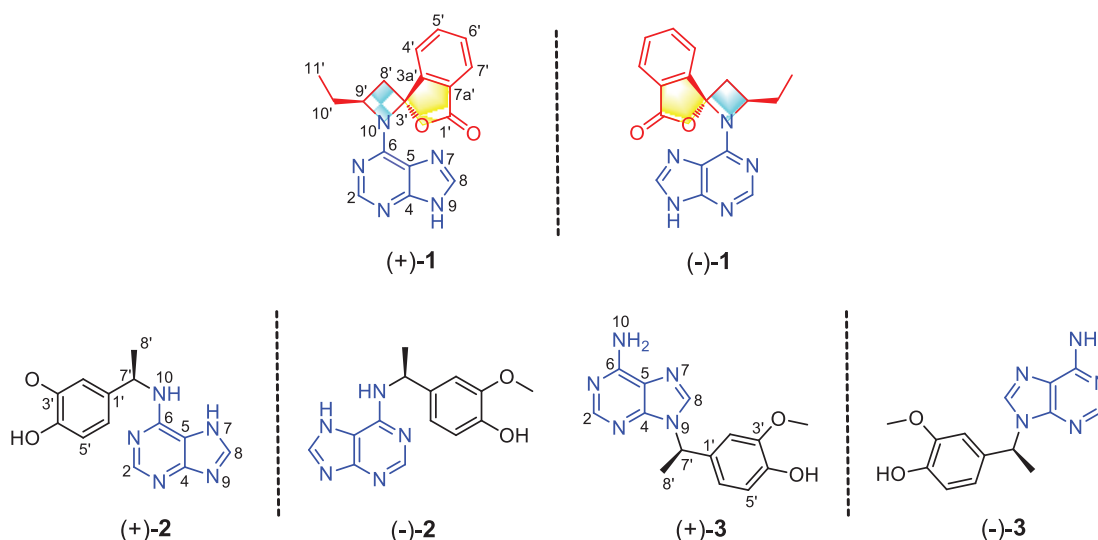
Fig. 1 Structures of compounds **1**–**3**.

by evaporating the water extract was suspended in warm water and partitioned with *n*-BuOH. The *n*-BuOH portion (9.3 kg) was separated by column chromatography on D101 macroporous adsorption resin, and six fractions were eluted with H_2O, 10%, 30%, 50%, 70%, and 95% ethanol. The 30% EtOH fraction (701.0 g) was further separated by elution on strong acid cation exchange resin with H_2O, 75% EtOH, and 75% EtOH containing 2 M ammonia. Of the three major fractions obtained, the one eluted with 75% EtOH containing 2 M ammonia water (120.0 g) was further separated into nine fractions (F_1–F_9) by silica gel column chromatography using gradient elution with CH_2Cl_2/MeOH (100:0–0:100). Separation of the F_6 fraction (3.1 g) by RP-MPLC (gradient elution with 10:90–100:0 MeOH/H_2O) afforded nine subfractions (F_{6-1}–F_{6-9}).

The F_{6-3} subfraction was further separated on a Sephadex LH-20 column (85% MeOH in H_2O), and seven subfractions F_{6-3-1}–F_{6-3-7} were obtained. F_{6-3-3} was successively purified by Sephadex LH-20 column chromatography (CH_2Cl_2/MeOH, 1:1), preparative TLC (CH_2Cl_2/MeOH, 9:1), and semipreparative HPLC (25% MeOH in H_2O) to yield compound **1** (1.5 mg). In addition, compounds **2** (6.3 mg) and **3** (3.2 mg) were obtained by purifying F_{6-3-4} on a silica gel column (CH_2Cl_2/MeOH, 80:1–1:1), followed by semipreparative HPLC (40% MeOH in H_2O).

Since compounds **1**–**3** show no cotton effects in their ECD spectra, and since their specific optical rotations are close to zero, these compounds were subjected to HPLC enantioseparation on a Daicel Chiralpak IG column or a Daicel Chiralpak AD-H column. Accordingly, three pairs of enantiomers, (+)-**1** (0.59 mg)/(−)-**1** (0.61 mg), (+)-**2** (2.60 mg)/(−)-**2** (2.50 mg), and (+)-**3** (1.54 mg)/(−)-**3** (1.60 mg), were obtained (Table 1).

2.4. Physicochemical properties and spectroscopic data of compounds 1–3

2.4.1. (+)-Liguadenine A and (−)-liguadenine A [(+)-1 and (−)-1]:

white amorphous powder; $\{[\alpha]_D^{25}$ +40.0 (*c* 0.04, MeOH); ECD (MeCN) λ_{max} ($\Delta\varepsilon$) 201 (−0.37), 219 (+9.45), 237 (+0.95), 279 (+1.29) nm; (+)-**1**}; $\{[\alpha]_D^{25}$ −47.5 (*c* 0.04, MeOH); ECD (MeCN) λ_{max} ($\Delta\varepsilon$) 201 (+1.29), 219 (−9.70), 237 (−0.51), 280 (−1.02) nm; (−)-**1**}; UV (MeCN) λ_{max} (log ε) 198 (4.44), 278 (3.68) nm; IR(ATR) ν_{max} 3030, 2920, 1769, 1716, 1618, 1571, 1466, 1400, 1285, 1264, 1085, 916, 797, 767, 735, 691 cm^{-1}; ^{1}H NMR (600 MHz, CD_3OD) and ^{13}C NMR (150 MHz, CD_3OD) data see Table 2; HR-ESI-MS *m/z*: 344.1126 [M + Na]$^+$, calcd. for $C_{17}H_{15}N_5O_2Na$, 344.1123.

2.4.2. (+)-Liguadenine B and (−)-liguadenine B [(+)-2 and (−)-2]:

colorless crystals; m.p. 148–149 °C; $\{[\alpha]_D^{25}$ +60.2 (*c* 0.07, MeOH); ECD (MeCN) λ_{max} ($\Delta\varepsilon$) 200 (+35.71), 214 (−21.93), 281 (+5.67) nm; (+)-**2**}; $\{[\alpha]_D^{25}$ −58.6 (*c* 0.06, MeOH); ECD (MeCN) λ_{max} ($\Delta\varepsilon$) 200 (−22.49), 214 (+13.87), 281 (−3.66) nm; (−)-**2**}; UV (MeCN) λ_{max} (log ε) 200 (4.22), 268 (3.72) nm; IR(ATR) ν_{max} 3362, 3334, 2975, 2944, 1613, 1521, 1454, 1431, 1260, 1224, 1138, 1055, 1009, 900, 851, 796, 707 cm^{-1}, ^{1}H NMR (600 MHz, CD_3OD) and ^{13}C NMR (150 MHz, CD_3OD) data see Table 2; HR-ESI-MS *m/z*: 308.1127 [M + Na]$^+$; calcd. for $C_{14}H_{15}N_5O_2Na$, 308.1123.

2.4.3. (+)-Liguadenine C and (−)-liguadenine C [(+)-3 and (−)-3]:

white amorphous powder; $\{[\alpha]_D^{25}$ +20.1 (*c* 0.06, MeOH); ECD (MeCN) λ_{max} ($\Delta\varepsilon$) 202 (+6.83), 253 (−0.85) nm; (+)-**3**}; $\{[\alpha]_D^{25}$ −14.7 (*c* 0.05, MeOH); ECD (MeCN) λ_{max} ($\Delta\varepsilon$) 201 (−5.51), 252 (+0.71) nm; (−)-**3**}; UV (MeCN) λ_{max} (log ε) 202 (3.70), 261 (2.98) nm; IR(ATR) ν_{max} 3327, 3178, 3125, 1643, 1515, 1466, 1276, 1212, 1027, 975, 853, 798, 708 cm^{-1}; ^{1}H NMR (600 MHz, CD_3OD) and ^{13}C NMR (150 MHz, CD_3-OD) data see Table 2; HR-ESI-MS *m/z*: 308.1106 [M + Na]$^+$, calcd. for $C_{14}H_{15}N_5O_2Na$, 308.1123.

2.5. X-ray crystallography data of compound 2

Compound **2** was dissolved with dichloromethane/methanol (4:6, V/V) and then slowly evaporated to a single crystal at 4°C. Crystal data for **2**: $C_{14}H_{15}N_5O_2 \cdot H_2O$, M = 303.32, tri-

Table 1 Chiral separation of racemic mixtures **1–3**.

Compound		Chiral phase	Mobile phase	Flow rate (mL/min)	Retention time (min)	Amount (mg)	Peak area ratio [(+)/(−)]
1	(+)-**1**	IG	MeOH/H_2O, 19:1	1.0	12.9	0.59	0.96/1
	(−)-**1**				10.2	0.61	
2	(+)-**2**	AD-H	n-hexane/ethanol, 10:1	1.0	31.4	2.60	1.04/1
	(−)-**2**				36.4	2.50	
3	(+)-**3**	AD-H	n-hexane/ethanol, 2:1	1.0	21.1	1.54	0.97/1
	(−)-**3**				24.2	1.60	

Table 2 NMR data of compounds **1–3** in CD$_3$OD (δ in ppm, J in Hz).

Position	1		2		3	
	^{1}H	^{13}C	^{1}H	^{13}C	^{1}H	^{13}C
2	8.40 s	153.7	8.22 s	153.8	8.21 s	153.6
4	—	160.7	—	151.3	—	150.4
5	—	113.9	—	118.8	—	120.2
6	—	151.8	—	154.7	—	157.3
8	8.60 s	145.7	8.08 s	140.6	8.17 s	140.9
1′	—	169.9	—	136.8	—	133.1
2′	—	—	7.03 s	111.2	7.00 d (2.4)	111.7
3′	—	95.3	—	149.0	—	149.3
3a′	—	151.8	—	—	—	—
4′	7.85 d (7.2)	123.8	—	146.7	—	147.8
5′	7.90 t (7.2)	136.6	6.75 d (7.8)	116.2	6.77 d (8.4)	116.4
6′	7.75 t (7.2)	132.2	6.88 d (7.8)	119.7	6.84 dd (8.4, 2.4)	120.3
7′	7.94 d (7.2)	126.6	5.43 m	51.0	5.80 q (7.2)	55.4
7a′	—	126.4			—	—
8′	3.20 dd (15.6, 11.4)	43.3	1.60 d (7.2)	23.1	1.95 d (7.2)	21.2
	2.57 dd (15.6, 1.8)					
9′	4.97 m	56.5	—	—	—	—
10′	2.37 m	26.6	—	—	—	—
	2.22 m					
11′	0.97 t (7.2)	7.8	—	—	—	—
OMe-3′	—	—	3.84 s	56.4	3.82 s	56.4

clinic, a = 7.8867(2) Å, b = 8.9792(2) Å, c = 11.4775(3) Å, α = 81.829(10)°, β = 73.211(10)°, γ = 68.117(10)°, V = 721.54(3) Å^3, space group P-1, T = 293(2) K, Z = 2, μ(Cu Kα) = 0.845 mm^{-1}, 22,147 reflections measured, 2652 independent reflections (R_{int} = 0.0765), average redundancy 8.351, completeness = 99.5 %. Final R indices ($I > 2\sigma(I)$): R_1 = 0.0428, wR_2 = 0.1140. Final R indices (all data): R_1 = 0.0637, wR_2 = 0.1256. The goodness of fit on F^2 was 1.073. CCDC number: 2157588. The results of X-ray diffraction analysis showed that **2** is an enantiomeric racemate.

2.6. Bioactivity assays

2.6.1. ELISA for TNF-α and IL-6

RAW264.7 cells were cultured according to a previously described method (Li et al., 2021), then they were dispensed into a 24-well plate at the density of 2×10^6 cells per well. After incubation at 37 °C for 24 h, the cells were treated with 1 μg/mL LPS for 24 h, with or without the tested compounds (12.5, 25, and 50 μM). The collected cell supernatants were spun at 1000 × g for 20 min to remove the particulate matter, then the levels of TNF-α and IL-6 in each sample were mea-

sured according to the manufacturer's instructions. In addition, the cytotoxic effects of the compounds on RAW264.7 cells were evaluated by CCK-8 assay. Curcumin was used as a positive control (1.56, 3.13, 6.25, 12.5, and 25 μM).

2.6.2. RNA extraction and RT-qPCR analysis

Cultured RAW264.7 cells were dispensed into 6-well plates. After 24 h treatment, the supernatant was removed, and the cells were washed twice with PBS. Subsequently, the total RNA was extracted and dissolved in 75 μL of RNase-free ddH$_2$O. The purity of total RNA was assessed by measuring the value of OD260/280 using a Nucleic Acid/Protein Analyzer. A 2 × RT OR-Easy^{TM} Master Premix reverse transcription kit was used to reverse-transcribe the RNA, and the obtained target cDNA was quantified using the EvaGreen 2 × qPCR MasterMix- No Dye kit, according to the manufacturer's instructions. Primers used for RT-qPCR see Table 3.

2.6.3. Other activity assay

The inhibitory effects of the isolates against OT-induced contractions of rat uterine smooth muscle (Liu et al., 2022, Ni et al., 2021), KCl-induced contractions of rat aorta rings

(Chen et al., 2022, Liu et al., 2019), and ADP-induced rabbit platelet aggregation (Pu et al., 2019) were measured as described previously.

3. Results and discussion

3.1. Structure elucidation

Compound **1** was isolated as a white amorphous powder. Its HR-ESI-MS presents a positive quasi-molecular ion at m/z 344.1126 (calcd. for $C_{17}H_{15}N_5O_2Na$, 344.1123), which suggests that the molecular formula of this compound is $C_{17}H_{15}N_5O_2$ possessing 13 degrees of unsaturation. The ^1H NMR and $^1H–^1H$ COSY data (Table 2 and Fig. 2) suggest that compound **1** possesses an adenine moiety [δ_H 8.40 (1H, s, H-2) and 8.60 (1H, s, H-8)] (Li et al., 2009), an *ortho*-substituted benzene ring [δ_H 7.94 (1H, d, J = 7.2 Hz, H-7′), 7.90 (1H, t, J = 7.2 Hz, H-5′), 7.85 (1H, d, J = 7.2 Hz, H-4′), and 7.75 (1H, t, J = 7.2 Hz, H-6′)], and a substituted *n*-butyl unit [δ_H 3.20 (1H, dd, J = 15.6, 11.4 Hz, H-8′a), 2.57 (1H, dd, J = 15.6, 1.8 Hz, H-8′b), 4.97 (1H, m, H-9′), 2.37 (1H, m, H-10′a), 2.22 (1H, m, H-10′b), and 0.97 (3H, t, J = 7.2 Hz, H$_3$-11′)]. The ^{13}C NMR (Table 2) and DEPT spectra show 17 carbon signals corresponding to the above units, with seven quaternary carbons, three of which (δ_C 160.7, 151.8, 113.9) are attributed to the adenine unit. The remaining four quaternary carbons include a carbonyl carbon (δ_C 169.9), two aromatic carbons (δ_C 151.8 and 126.4), and a carbon (δ_C 95.3) bonded to two hetero atoms. The resonance signals detailed above reveal that compound **1** is an unusual hybrid phthalide–adenine. The HMBC correlations (Fig. 2) of H-2 with C-4 and C-6; and H-8 with C-4 and C-5 confirm the presence of an adenine unit. Meanwhile, the *n*-butylphthalide fragment is evidenced by the HMBC correlations of H-4′ with C-3′, C-6′, and C-7a′; H-5′ with C-3a′ and C-7; H-6′ with C-4′ and C-

7a′; H-7′ with C-1′, C-3a′, and C-5′; and H-8′ with C-3′, C-3a′, C-9′, and C-10′, as well as by the $^1H–^1H$ COSY signals of H-4′/H-5′/H-6′/H-7′ and H-8′/H-9′/H-10′/H-11′. The adenine and butylphthalide units of **1** account for 12 degrees of unsaturation. The 13th degree of unsaturation suggests a ring linkage between the two units. In addition, compared to the common *n*-butylphthalide compound, C-3′ in compound **1** is changed to a quaternary carbon (δ_C 95.3) bonded to two hetero atoms, while C-9′ in compound **1** is changed to a CH group (δ_H 4.97, δ_C 56.5) linked to a N atom. Overall, the spectroscopic data indicate that a C-3′–N-10–C-9′ linkage between the adenine and butylphthalide units in **1** forms a four-membered aza-heterocycle, resulting in the formation of a rare 5-oxa-1-azaspiro[3,4]octane moiety. Based on these results, the planar structure of compound **1** is established.

The relative configuration of compound **1** was elucidated based on the analysis of NOESY cross-peaks. The NOESY correlations of H-4′ (δ_H 7.85)/H-8′a (δ_H 3.20) and H-8′a (δ_H 3.20)/H-10′a (δ_H 2.37) demonstrate that H-4′, H-8′a, and H-
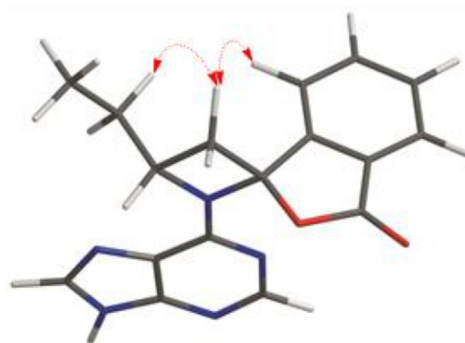
Fig. 3 Key NOESY correlations of compound **1**.

Table 3 Primers used for RT-qPCR.

Primers	Forward (5′→3′)	Reverse (5′→3′)
GAPDH	GGCCTTCCGTGTTCCTACC	TGCCTGCTTCACCACCTTC
TNF-α	ATGAGAAGTTCCCAAATGGC	CTCCACTTGGTGGTTTGCTA
IL-6	GGGACTGATGCTGGTGACAA	TCCACGATTTCCCAGAGAACA

1   **2**   **3**

— ^1H-^1H COSY   ⌒ HMBC

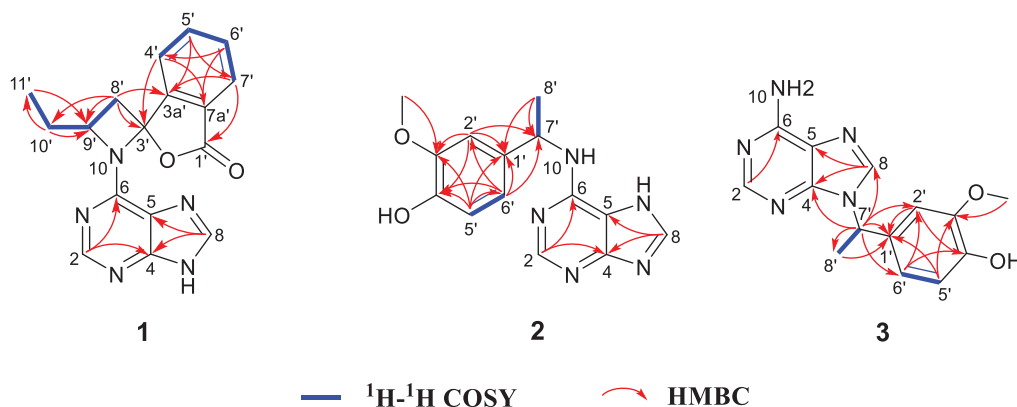**Fig. 2** Key $^1H–^1H$ COSY and HMBC correlations of compounds **1–3**.
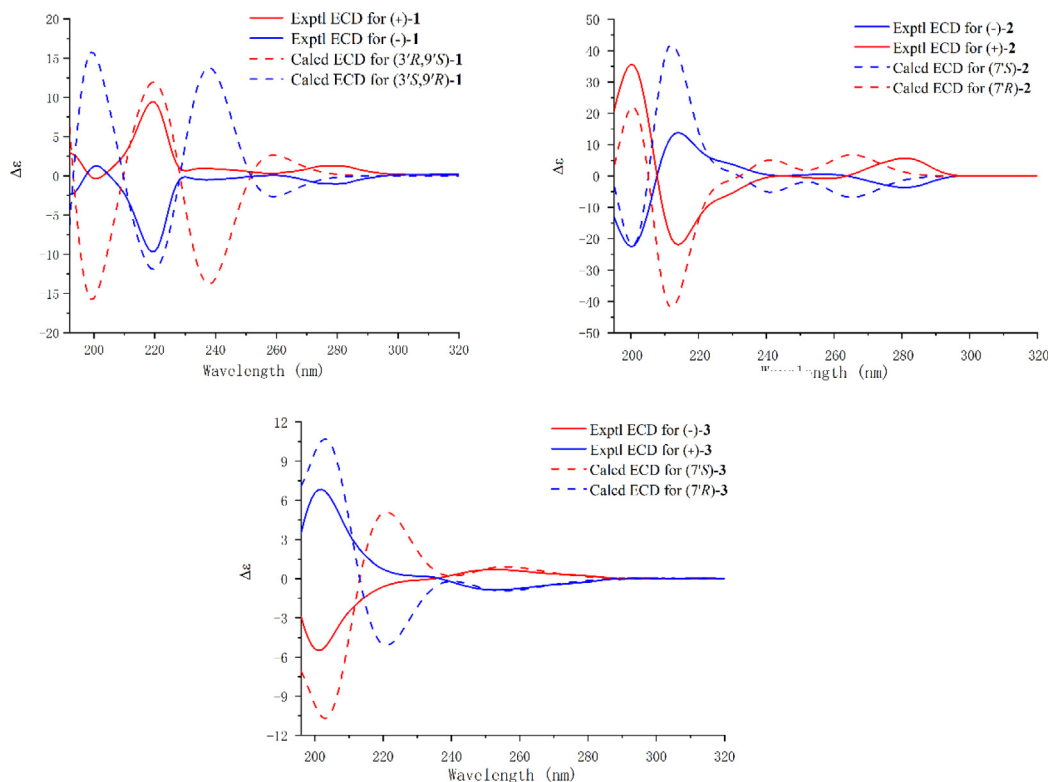
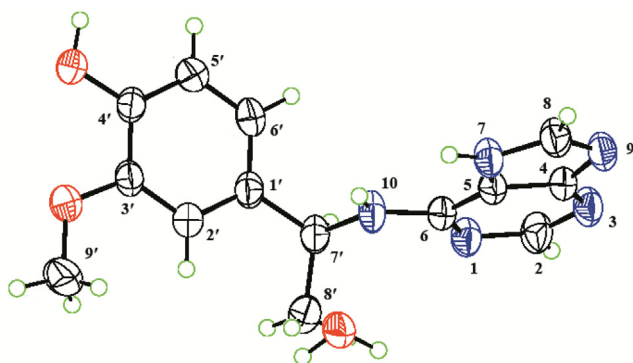**Fig. 4**   The experimental and calculated ECD spectra of compounds **1**–**3**.

Fig. 5   X-ray crystallographic structure of compound **2**.

10′ have the same orientation (Fig. 3). Interestingly, no cotton effect is observed in ECD spectrum of compound **1**, which suggests that this compound may be a racemic mixture. Indeed, chiral separation of **1** on a Daicel Chiralpak IG column yields (+)-**1** and (−)-**1** (Table 1), and based on the comparison of experimental and calculated ECD spectra, the absolute configurations of these enantiomers are 3′R,9′S and 3′S,9′R, respectively (Fig. 4). Hence, (+)-**1** and (−)-**1** were established as (+)-(3′R,9′S)-liguadenine A and (−)-(3′S,9′R)-liguadenine A, respectively.

Based on HR-ESI-MS analysis (m/z 308.1127 [M + Na]$^+$, calcd. for C$_{14}$H$_{15}$N$_5$O$_2$Na, 308.1123), the molecular formula of compound **2** is C$_{14}$H$_{15}$N$_5$O$_2$. ^{1}H and ^{13}C NMR analyses reveal that **2** is an adenine hybrid that comprises a 4-ethyl-2-methoxyphenol moiety with C-7′ substituted [δ_H 7.03 (1H, s,

H-2′), 6.88 (1H, d, J = 7.8 Hz, H-6′), 6.75 (1H, d, J = 7.8 Hz, H-5′), 5.43 (1H, m, H-7′), and 1.60 (3H, d, J = 7.2 Hz, H-8′); δ_C 149.0, 146.7, 136.8, 119.7, 116.2, 111.2, 51.0, and 23.1], as well as a methoxy group [δ_H 3.84 (3H, s, OMe-3′); δ_C 56.4]. This is confirmed by the HMBC correlations of H-2′ with C-1′, C-3′, C-4′, and C-7′; OMe-3′ with C-3′; H-6′ with C-1′, C-2′, C-4′, and C-7′; and H$_3$-8′ with C-1′ and C-7′, together with the ^{1}H–^{1}H COSY correlations of H-5′/H-6′ and H-7′/H-8′ (Fig. 2). Although no HMBC correlation of H-7′/C-6 is observed, the adenine and 4-ethyl-2-methoxyphenol substructures must be connected by a C-6–N-10–C-7′ linkage in order to match the molecular formula and chemical shifts of C-6 and C-7′. This linkage is verified by X-single crystal diffraction analysis (Fig. 5). Considering that the specific optical rotation of **2** is zero, this compound was subjected to enantioseparation on a Daicel Chiralpak AD-H column (Table 1). As described for compound **1**, ECD calculations were used to determine the absolute configuration of **2**, and as shown in Fig. 4, the experimental ECD spectra of (+)-**2** and (−)-**2** are consistent with the calculated ECD spectra of (7′R)-**2** and (7′S)-**2**, respectively. Therefore, compounds (+)-**2** and (−)-**2** are labelled (+)-(7′R)-liguadenine B and (−)-(7′S)-liguadenine B.

The spectroscopic data of compound **3** are similar to those of **2**. Indeed, HR-ESI-MS analysis reveals that the two compounds possess the same molecular formula, which indicates that they are isomers. The ^{1}H and ^{13}C NMR data of **3** (Table 2) suggest that this compound is also a hybrid, and that it is composed of adenine and 4-ethyl-2-methoxyphenol moieties, like compound **2**. However, the C-4, C-5, C-6, C-1′, C-7′, and C-8′ resonances in the ^{13}C NMR spectrum of **3** are shifted by $\Delta\delta_C$ −0.9, +1.4, +2.6, −3.7, +4.4, and −1.9 ppm, respec-
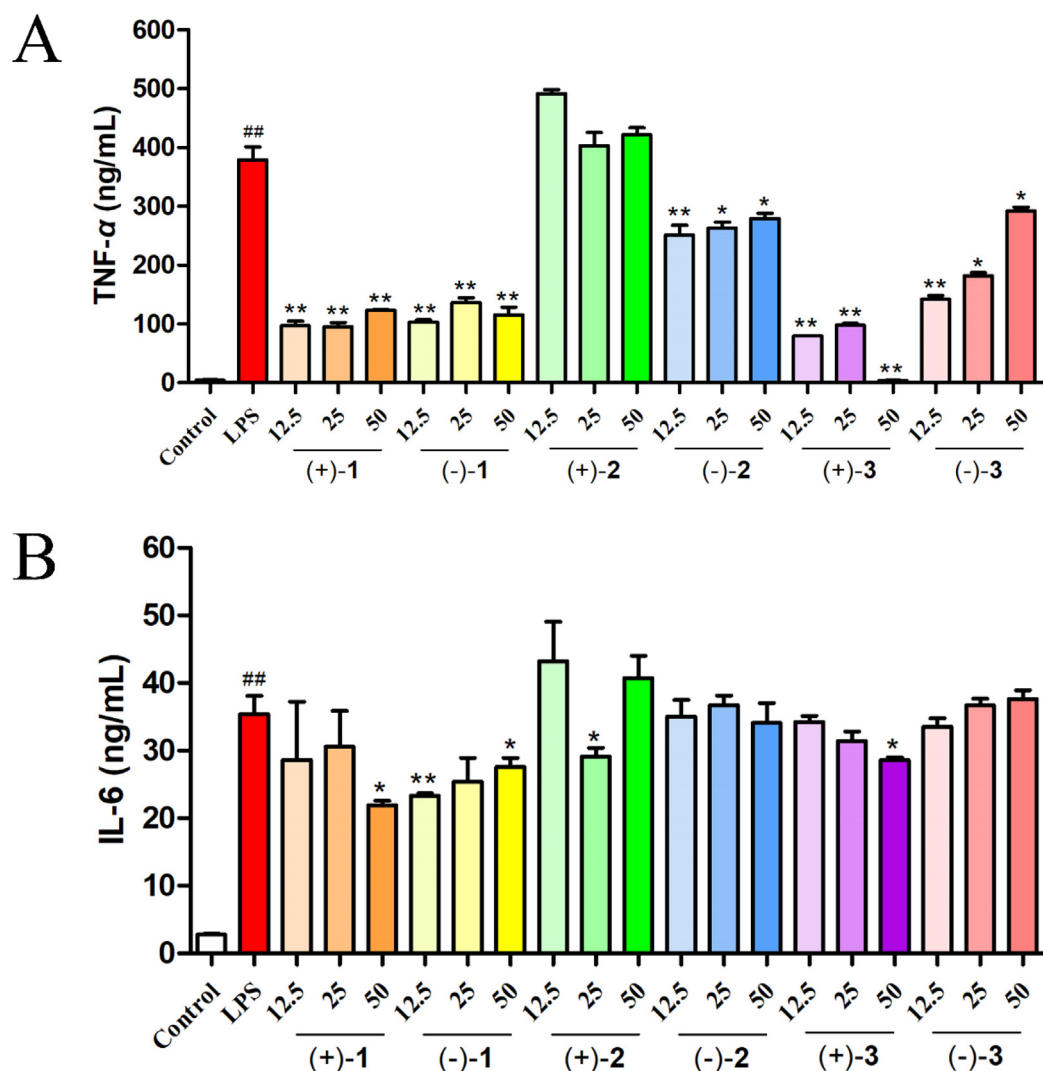
Fig. 6 Effects of compounds **1**–**3** on the levels of TNF-α (A) and IL-6 (B) in LPS-stimulated RAW 264.7 cells. The data represent the mean $\pm$ SD of three experiments. $^{\#\#}P < 0.01$ vs the control group; $^{*}p < 0.05$, $^{**}p < 0.01$ vs the LPS group.
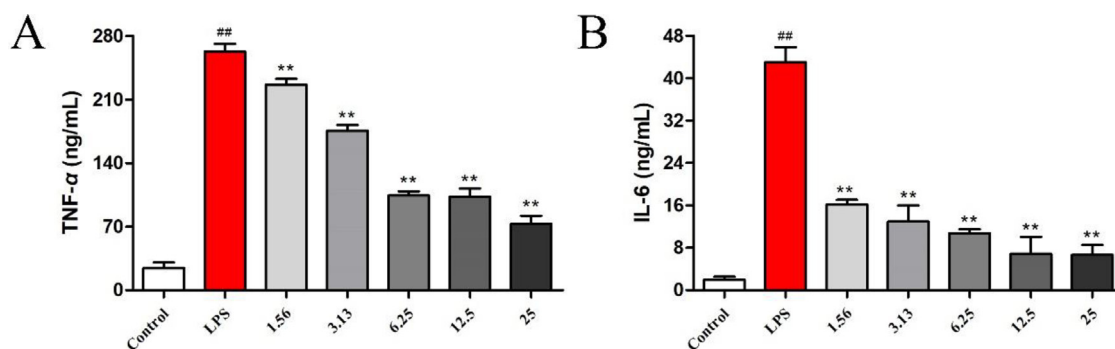

Fig. 7 Effects of curcumin on the levels of TNF-α (A) and IL-6 (B) in LPS-stimulated RAW 264.7 cells. The data represent the mean $\pm$ SD of three experiments. $^{\#\#}P < 0.01$ vs the control group; $^{**}p < 0.01$ vs the LPS group.

tively, compared to the same signals in the spectrum of **2**. Therefore, the difference between compounds **3** and **2** lies in the linkage between the two moieties. Based on the HMBC correlations of H-7′ with C-4, C-8, C-1′, C-2′, C-6′, and C-8′, the adenine and 4-ethyl-2-methoxyphenol substructures in **3** are connected by a N-9–C-7′ linkage. The specific optical rota-
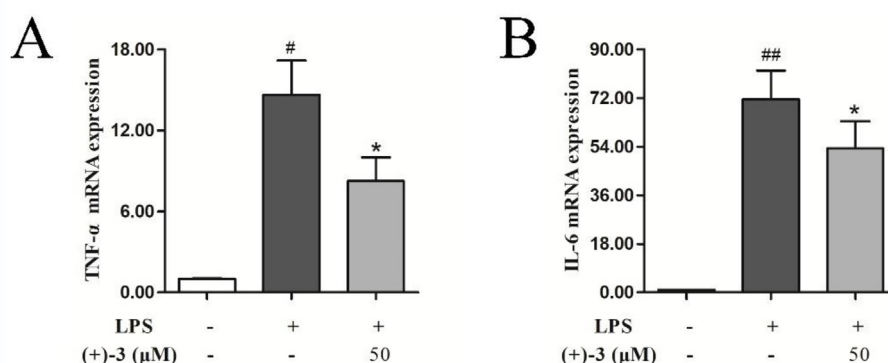
Fig. 8 Effects of compound (+)-**3** on the mRNA expression of TNF-α (A) and IL-6 (B) in LPS-stimulated RAW264.7 cells. The data represent the mean ± SD of three experiments. $^{\#}P < 0.05$, $^{\#\#}P < 0.01$ vs the control group; $^{*}p < 0.05$, vs the LPS group.

tion and ECD spectrum of **3** suggest that it is a racemic mixture, and the absolute configurations of the separated (+)-**3** and (−)-**3** enantiomers are $7'R$ and $7'S$, respectively, as determined by ECD calculations (Fig. 4). Therefore, compounds (+)-**3** and (−)-**3** are established as (+)-($7'R$)-liguadenine C and (−)-($7'S$)-liguadenine C, respectively.

3.2. Effects of compounds 1–3 on TNF-α and IL-6 levels in RAW 264.7 cells

First, all compounds showed no cytotoxic activity against RAW264.7 cells in the range of experimental concentrations. Then, the anti-inflammatory effects of the three pairs of enantiomeric alkaloids isolated from *L. chuanxiong* were assayed using LPS-stimulated RAW 264.7 macrophages, and the concentrations of inflammatory factors (TNF-α and IL-6) in the supernatant were detected by ELISA. Except for (+)-**2**, all compounds exhibit significant inhibitory activity against LPS-induced TNF-α production, with (+)-**3** being the most active (Fig. 6). Compounds (+)-**1**/(−)-**1** and (+)-**3** also show significant inhibitory effects against the production of IL-6. Interestingly, the anti-inflammatory activity of (+)-**3** is better than that of its enantiomer. In addition, a comparison of the anti-inflammatory effects of (±)-**2** and (±)-**3** indicates that the linkage between the adenine and paraethyl phenol moieties in these compounds plays an important role in anti-inflammatory activity (N-9 linkage > N-10 linkage). Curcumin was used as a positive control and showed a significant inhibitory effect on TNF and IL-6 release (Fig. 7).

3.3. Effect of compound (+)-3 on the mRNA expression of LPS-induced inflammatory cytokines in RAW264.7 cells

The effect of (+)-**3**, the most active compound, on the mRNA expression of LPS-induced inflammatory cytokines in RAW264.7 cells was further explored. As shown in Fig. 8, LPS prominently induces the mRNA expressions of TNF-α and IL-6 compared to the normal control. However, treatment with 50 μM (+)-**3** significantly downregulates the IL-6 and TNF-α mRNA expressions induced by LPS. These results suggest that (+)-**3** suppresses inflammatory response by downregulating the mRNA expressions of TNF-α and IL-6.

3.4. Other activity assay

None of the tested compounds showed inhibitory effects against OT-induced contractions of rat uterine smooth muscle, KCl-induced contractions of rat aorta rings, and ADP-induced rabbit platelet aggregation.

4. Conclusion

In summary, three pairs of new enantiomeric adenine hybrids (**1**–**3**) were isolated from the rhizome of *L. chuanxiong*. (+)/(−)-Liguadenines B and C [(+)/(−)-**2** and **3**] are unusual hybrid paraethyl phenol–adenines, while (+)/(−)-liguadenine A [(+)/(−)-**1**] are novel hybrid phthalide–adenines possessing a rare 5-oxa-1-azaspiro[3,4] octane moiety. Compounds (+)/(−)-**1** and (+)-**3** exert anti-inflammatory effects by inhibiting the production of TNF-α and IL-6 in LPS-stimulated RAW264.7 cells. In addition to enriching the literature with data concerning rare types of alkaloids in *L. chuanxiong*, this study provides a reference for the research of anti-inflammatory compounds in *L. chuanxiong*.

Declaration of Competing Interest

The authors declare that they have no known competing financial interests or personal relationships that could have appeared to influence the work reported in this paper.

Appendix A. Supplementary data

https://doi.org/10.1016/j.arabjc.2022.xxxxxx

Supplementary data to this article can be found online at https://doi.org/10.1016/j.arabjc.2023.104696.

References

Araya, J.J., Zhang, H., Prisinzano, T.E., Mitscher, L.A., Timmermann, B.N., 2011. Identification of unprecedented purine-containing compounds, the zingerines, from ginger rhizomes (*Zingiber officinale* Roscoe) using a phase-trafficking approach. Phytochemistry 72, 935–941. https://doi.org/10.1016/j.phytochem.2011.03.007.

Bakr, R.O., El-Behairy, M.F., Elissawy, A.M., Elimam, H., Fayed, M. A.A., 2021. New adenosine derivatives from *Aizoon canariense* L.: in vitro anticholinesterase, antimicrobial, and cytotoxic evaluation of its extracts. Molecules 26, 1198. https://doi.org/10.3390/molecules26051198.

Buyens, D.M.S., Mangondo, P., Cukrowski, I., Pilcher, L.A., 2017. Solvent-directed regioselective benzylation of adenine: characterization of N9-benzyladenine and N3-benzyladenine. J. Heterocyclic Chem. 54, 2946–2950. https://doi.org/10.1002/jhet.2894.

Capraro, H.G., Winkler, T., Martin, P., 1983. [2 + 2]-Cycloaddition of 'maleic isoimides' with ketenes and conversion of spiro-β-lactams to muconic and tetramic acid derivatives. Helv. Chim. Acta 66, 362–378.

Chen, J.F., Liu, F., Qiao, M.M., Shu, H.Z., Li, X.C., Peng, C., Xiong, L., 2022. Vasorelaxant effect of curcubisabolanin A isolated from *Curcuma longa* through the PI3K/Akt/eNOS signaling pathway. J. Ethnopharmacol. 294,. https://doi.org/10.1016/j.jep.2022.115332 115332.

Chen, Z., Zhang, C., Gao, F., Fu, Q., Fu, C., He, Y., Zhang, J., 2018. A systematic review on the rhizome of *Ligusticum chuanxiong* Hort. (Chuanxiong). Food Chem. Toxicol. 119, 309–325. https://doi.org/10.1016/j.fct.2018.02.050.

Cordero, F.M., Vurchio, C., Brandi, A., Gandolfi, R., 2011. Mechanism of the acid-mediated thermal fragmentation of 5-spirocyclobutane-isoxazolidines. Eur. J. Org. Chem. 28, 5608–5616. https://doi.org/10.1002/ejoc.201100621.

Goswami, M., Wilke, K.E., Carlson, E.E., 2017. Rational design of selective adenine-based scaffolds for inactivation of bacterial histidine kinases. J. Med. Chem. 60, 8170–8182. https://doi.org/10.1021/acs.jmedchem.7b01066.

Huang, L., Peng, C., Guo, L., Feng, R., Shu, H.Z., Tian, Y.C., Zhou, Q.M., Xiong, L., 2022. Six pairs of enantiomeric phthalide dimers from the rhizomes of *Ligusticum chuanxiong* and their absolute configurations and anti-inflammatory activities. Bioorg. Chem. 127,. https://doi.org/10.1016/j.bioorg.2022.105970 105970.

Li, Y.Y., Chou, G.X., Wang, Z.T., 2009. Chemical constituents in n-butanol extract from the seeds of *Alpinia katsumadai*. Chin. J. Nat. Med. 7, 417–420. https://doi.org/10.3724/SP.J.1009.2009.00417.

Li, X.R., Liu, J., Peng, C., Zhou, Q.M., Liu, F., Guo, L., Xiong, L., 2021. Polyacetylene glucosides from the florets of *Carthamus tinctorius* and their anti-inflammatory activity. Phytochemistry 187,. https://doi.org/10.1016/j.phytochem.2021.112770 112770.

Liu, J., Feng, R., Dai, O., Ni, H., Liu, L.S., Shu, H.Z., Lu, Y., Peng, C., Xiong, L., 2022. Isoindolines and phthalides from the rhizomes of *Ligusticum chuanxiong* and their relaxant effects on the uterine smooth muscle. Phytochemistry 198,. https://doi.org/10.1016/j.phytochem.2022.113159 113159.

Liu, Y., Liu, F., Qiao, M.M., Guo, L., Chen, M.H., Peng, C., Xiong, L., 2019. Curcumanes A and B, two bicyclic sesquiterpenoids with significant vasorelaxant activity from *Curcuma longa*. Org. Lett. 21, 1197–1201. https://doi.org/10.1021/acs.orglett.9b00149.

Luo, Z., Jiang, Z., Jiang, W., Lin, D., 2018. C−H amination of purine derivatives via radical oxidative coupling. J. Org. Chem. 83, 3710–3718. https://doi.org/10.1021/acs.joc.8b00066.

Ma, H.Y., Sun, Y., Zhou, Y.Z., Hong, M., Pei, Y.H., 2008. Two new constituents from *Artemisia capillaris* Thunb. Molecules 13, 267–271. https://doi.org/10.3390/molecules13020267.

Ma, M., Zhao, J., Wang, S., Li, S., Yang, Y., Shi, J., Fan, X., He, L., 2007. Bromophenols coupled with nucleoside bases and brominated tetrahydroisoquinolines from the red alga *Rhodomela confervoides*. J. Nat. Prod. 70, 337–341. https://doi.org/10.1021/np060400l.

Ni, H., Liu, J., Dai, O., Feng, R., Liu, F., Cao, X.Y., Peng, C., Xiong, L., 2021. Chemical composition and uterine smooth muscle relaxant activity of essential oils from 10 kinds of blood-activating and stasis-resolving Chinese medicinal herbs. J. Ethnopharmacol. 269,. https://doi.org/10.1016/j.jep.2020.113713 113713.

Pu, Z.H., Liu, J., Peng, C., Luo, M., Zhou, Q.M., Xie, X.F., Chen, M. H., Xiong, L., 2019. Nucleoside alkaloids with anti-platelet aggregation activity from the rhizomes of *Ligusticum striatum*. Nat. Prod. Res. 33, 1399–1405. https://doi.org/10.1080/14786419.2017.1416382.

Pu, Z.H., Dai, M., Xiong, L., Peng, C., 2022. Total alkaloids from the rhizomes of *Ligusticum striatum*: a review of chemical analysis and pharmacological activities. Nat. Prod. Res. 36, 3489–3506. https://doi.org/10.1080/14786419.2020.1830398.

Roth, M., 1979. Spiro-β-lactame durch [2 + 2]-cycloaddition von ketenen an iminolactone. Helv. Chim. Acta 62, 1966–1977. https://doi.org/10.1002/hlca.19790620625.

Shipov, A.G., Baukov, Y.I., 1988. Cheminform abstract: reaction of spiro-β-lactams, e.g. (I), with O-silyl substituted enols (II). ChemInform 19, 46.

Wang, W., Fang, S., Xiong, Z., 2019. Protective effect of polysaccharide from *Ligusticum chuanxiong* hort against H_2O_2-induced toxicity in zebrafish embryo. Carbohydr. Polym. 221, 73–83. https://doi.org/10.1016/j.carbpol.2019.05.087.

Wang, Z.W., Wang, Y.L., Zhang, J.P., Wei, Q.H., Wang, X.J., 2021. Monoterpene indole alkaloids from the roots of *Bousigonia mekongensis* and their anti-diabetic nephropathy activity. Fitoterapia 153,. https://doi.org/10.1016/j.fitote.2021.104964 104964.

Wang, J., Wang, L., Zhou, H., Liang, X.D., Zhang, M.T., Tang, Y.X., Wang, J.H., Mao, J.L., 2022. The isolation, structural features and biological activities of polysaccharide from *Ligusticum chuanxiong*: A review. Carbohydr. Polym. 285,. https://doi.org/10.1016/j.carbpol.2021.118971 118971.

Zhang, K., Fang, K.L., Wang, T., Xu, L.T., Zhao, Y., Wang, X.N., Xiang, L., Shen, T., 2021. Chemical constituents from the rhizome of *Ligusticum chuanxiong* Hort. and their Nrf2 inducing activity. Chem. Biodivers. 18, e2100302.

Zhang, X., Han, B., Feng, Z.M., Yang, Y.N., Jiang, J.S., Zhang, P.C., 2018a. Novel phenylpropanoid-amino acid adducts from *Ligusticum chuanxiong*. Org. Chem. Front. 5, 1423–1430. https://doi.org/10.1039/C8QO00012C.

Zhang, X., Han, B., Feng, Z.M., Yang, Y.N., Jiang, J.S., Zhang, P.C., 2018b. Ferulic acid derivatives from *Ligusticum chuanxiong*. Fitoterapia 125, 147–154. https://doi.org/10.1016/j.fitote.2018.01.005.

Zhang, X., Yan, H.W., Feng, Z.M., Yang, Y.N., Jiang, J.S., Zhang, P. C., 2020. Neophathalides A and B, two pairs of unusual phthalide analog enantiomers from *Ligusticum chuanxiong*. Org. Biomol. Chem. 18, 5453–5457. https://doi.org/10.1039/d0ob01014f.